Interaction Region for Detector-Machine Interface *

Toshiaki Tauchi
KEK,High Energy Accelerator Research Organization,
1-1 Oho, Tsukuba-shi,Ibaraki-ken, 305-0810, Japan.

Abstract

High luminosity upgrade scenario is briefly explained to be seriously considered in interaction region issues. The major progress of the interaction region is reported since the Beijing workshop, especially emphasizing the performance study of the pair monitor as a nano-meter beam size measurement. Finally, future direction toward higher solenoidal field is discussed with some proposals of detectors.

1 JLC parameters,A,X,Y

Recently K. Yokoya presented an upgraded scenario of increasing luminosity of JLC at $\sqrt{s} \leq 500$ GeV [1]. It can be realized with smaller beam sizes and higher beam currents. The upgraded parameter-sets (X,Y) are listed in Table 1, which are compared with the basic (A) and previous (JLC-DS [3]) sets, and with the most recent TESLA parameter-set at $\sqrt{s}$ =500GeV.

At the first upgrade step X from A , the number of bunches is increased from 95 to 190 and the bunch separation is decreased from 2.8ns to 1.4ns. Thus keeping the same pulse length, the bunch population is reduced from 0.75×10^{10} to 0.55×10^{10} for the reasonable positron generation. With an improvement of vertical emittance($\gamma\epsilon_y$) at the damping ring and a smaller emittance dilution in the linac, the horizontal beta function (β_x^*) is reduced from 10mm to 6mm at IP. As the result, the luminosity goes up by a factor of 1.8 while the beamstrahlung effects (δ_{BS}, n_γ) remain almost the same. At the next step Y from X, only the bunch population is increased from 0.55×10^{10} to 0.70×10^{10}. All the upgrades (A→X→Y) would yield a luminosity of $2.61 \times 10^{34}\mathrm{cm}^{-2}\mathrm{s}^{-1}$ which is 3 times as high as the basic (A) luminosity. However, this final step is very much challenging for the accelerator system because of heavy beam loadings and tighter tolerances in alignments of accelerating cavities.

There is another upgrade step Z from X at low energy of $\sqrt{s}$ <250GeV, if Y is too difficult for operating the accelerator. Since a beamstrahlung is not a problem in this energy region, the horizontal emittance ($\gamma\epsilon_x$) can be decreased to 1/3 of the basic one by a laser-Compton cooling [4] without no additional tolerance problem in the linac. The luminosity becomes 3.3 times higher than the A.

Figure 1 shows the upgraded (X,Y and Z) luminosities together with the basic one (A) at $120 < \sqrt{s} < 500$GeV.

*to be submitted to the proceedings of The Second ACFA Workshop on Physics/Detector at the Linear Collider, November 4 - 6, 1999 Korea University, Seoul, Korea

Table 1: JLC parameters(JLC-DS,A) including upgrades(X,Y) for high luminosity at $\sqrt{s}$=500GeV, together with TESLA parameters(May 1999), where a major improvement in A from JLC-DS is a bunch separation, that is 2.8ns for lower beam loading while it was 1.4ns in JLC-DS. Pinch and hour-glass effects are included in luminosities with a crab crossing at JLC.

parameter	unit	JLC-DS	A	X	Y	TESLA
Luminosity	$10^{34}/\mathrm{cm}^2\mathrm{s}$	0.83	0.88	1.57	2.61	3.2
RF frequency	GHz	11.4	11.4	11.4	11.4	1.3
Repetition rate	Hz	150	150	150	150	5
Bunch population	10^{10}	0.70	0.75	0.55	0.70	2.0
No. of bunches	/pulse	85	95	190	190	2820
Bunch separation	ns	1.4	2.8	1.4	1.4	337
Linac length	km /beam	5.4	5.21	5.54	5.97	15
Bunch length (σ_z)	μm	90	90	80	80	400
$\gamma\epsilon_x$ (IP)	10^{-6} m	3.3	4	4	4	10
$\gamma\epsilon_y$ (IP)	10^{-6} m	0.048	0.06	0.04	0.04	0.03
β_x^*	mm	10	10	6	6	15
β_y^*	mm	0.1	0.1	0.1	0.1	0.4
IP beam size (σ_x^*)	nm	260	286	222	222	553
IP beam size (σ_y^*)	nm	3.14	3.15	2.86	2.86	5.0
Energy loss (δ_{BS}) due to beamstrahlung(BS)	%	4.40	4.42	4.39	6.67	2.7
No. of BS photons (n_γ)	/ $\mathrm{e}^{-(+)}$	1.12	1.07	1.01	1.28	1.6

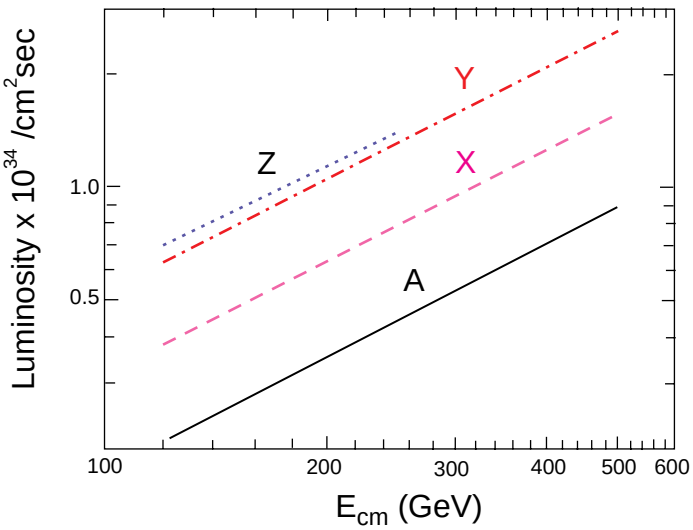

Figure 1: Luminosities as a function of center-of-mass energy($\sqrt{s}$), where A is the basic luminosity while X, Y and Z are upgraded ones (K.Yokoya, March 1999).

2 Beam delivery system and IP layout

The beam delivery system [3] comprizes collimation(1200m) and final focus(1600m) systems as shown in Fig. 2, which can deliver beams up to 750GeV corresponding to $\sqrt{s} = 1.5$TeV. There are two interaction points (IP) horizontally separated by large bending magnets (big bend's) of ±7m rad. At IP1, e^+ and e^- beams collide with ±4mrad crossing angle employing a crab crossing scheme. The second IP2 may be used for $\gamma\gamma$, $e\gamma$ as well as for the second e^+e^- collisions [7].

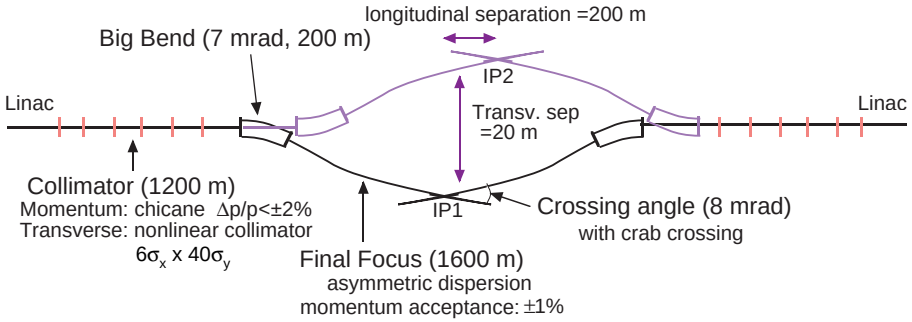

Figure 2: Schematic layout of the beam delivery system at JLC (JLC Design Study, April 1997).

IP layout is shown in Fig.3. Nearest final quadrupole magnet (QC1) is located at 2m from IP, where the QC1 is shielded against a solenoid field of 2 Tesla by a superconducting compensation magnet. A huge number of X rays, which are created in electromagnetic showers of $e^{\pm}$ pairs at QC1, are absorbed in conical and cylindrical tungsten masks. Angular coverage of the conical mask ranges from 0.15 to 0.2 radian, leaving a small dead cone angle, but the front part of the conical mask could be instrumented as a calorimeter. There is the luminosity monitor covering an angular region between 0.05 and 0.15 radian inside the mask. The carbon mask in front of the QC1 is very effective to absorb low energy back-scattered electrons. The 4-layer vertex detector (VTX) is located at radial distance from 2.4 to 6.0cm, followed by an intermediate tracker to link charged tracks between the CDC and the VTX. All these instruments are installed in a

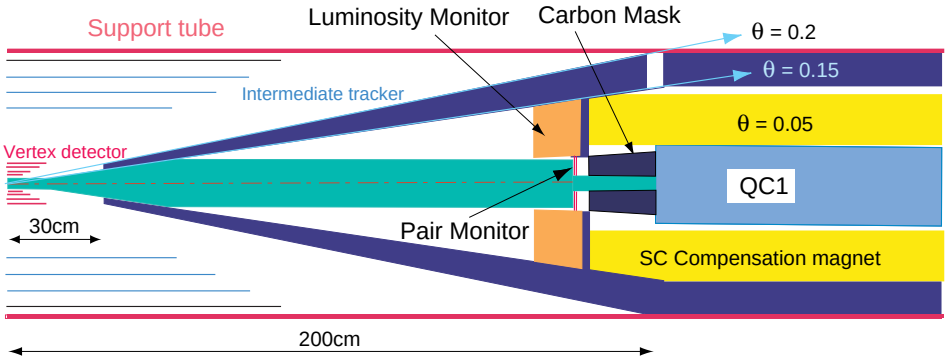

Figure 3: Interaction region.

support tube of 80cm diameter[9].

The interaction region has been updated since the 1st ACFA-LC (Beijing) workshop[8] in order to further reduce $e^{\pm}$ pair backgrounds in the vertex detector(VTX) and the central drift chamber (CDC), especially X-rays in the CDC. The major changes are in the beam pipes and the locations of the carbon mask and the pair monitor. The beam pipe inside the VTX is made of 0.5mm thick beryllium, 4cm in diameter, while the major part is a 15cm diameter beam pipe of 2mm thick aluminum in the mask. These two beam pipes are connected with a conical beryllium pipe of 2mm thickness. The 15 cm diameter is large enough for $e^{\pm}$ pair particles to curl inside the beam pipe without interactions. The pair monitors consisting of active pixel device are now located at 176cm from IP, i.e. inside of luminosity monitor(50 - 150 mrad). In the previous design, they were closer to IP and were one of the sources of X rays.

3 Performance of the pair monitor

The disk-shaped pair monitor comprizes double layers of active pixel sensors whose pixel size and thickness are $100 \times 100\mu\text{m}^2$ and 300μm of silicon, respectively. The inner and outer radii are 2 and 8.5cm, respectively. The pair monitor should measure positions and energy deposits of electrons or positrons and secondary photons. Figure 4 shows the energy deposits simulated with detailed geometries by JIM, where the pairs have been generated with beam parameters of JLC-A by CAIN21d[5]. Many of them hit only one cell and, as clearly seen in this figure, a very sharp peak appears around 100keV. Therefore, they can be effectively discriminated from the secondary backgrounds simply by a 70 keV threshold in energy deposits.

In order to see how we can measure the beam sizes, pairs have been generated with five different vertical beam sizes at IP by CAIN[5], *i.e.* $\sigma_y = \sigma_y^o$(basic), $2 \times \sigma_y^o$, $3 \times \sigma_y^o$, $4 \times \sigma_y^o$ and $10 \times \sigma_y^o$ for the statistics of 20, 40, 60 50 and 110 bunch crossings, respectively, while the other beam parameters are the same as the basic ones. The minimum energy of the pair particles was 3 MeV.

Radial distributions of the pairs are shown in Fig.5, where the number of hits are normalized at 20 bunch crossings for realistic statistical comparisons. All five histograms have sharp shoulders, while negligibly small tails are due to those scattered inherently at large angles. As clearly seen in this figure, positions of the shoulders do not depend on the vertical beam size(σ_y) indeed as described in [6]. Since they depend on the horizontal beam size(σ_x) as well as well-known beam intensities, the horizontal beam size can be estimated by the radial distribution.

The most interesting observable is the distribution of azimuthal angles, since the angles carry an information of the vertical beam size as a function of aspect ratio,$A \equiv \sigma_x/\sigma_y$. Among the pair particles, particles of the same charge as the oncoming beam must be deflected with large angles because of repulsive Coulomb forces. When the oncoming beam has a large aspect ratio, the particles are scattered asymmetrically due to the asymmetric Coulomb potential, that is, more vertically than horizontally. Figure 6 shows a scatter plot of hits in the pair monitor on a plane of azimuthal angle and radial position. Two dense bands can be seen, which are made of particles deflected upward or downward and swum helically in the 2 Tesla solenoid field. In order to quantify the asymmetry, we set four regions (H_2, L_1, H_1, L_2) as shown in Fig.6. Area of H_2 and L_2 is larger than that of H_1 and L_1 because of left-right asymmetry with 8 mrad crossing angle. Then, we defined a ratio, $R \equiv (L_1 + L_2)/(H_1 + H_2)$ as proposed[6], where L_1, L_2, H_1, H_2 represent the number of hits in each region. It is expected that R becomes smaller as A increases while $R = 1$ for round beams. The simulation results are shown for beams with five different σ_y's in Fig.7. Up to $4 \times \sigma_y^o$, we observed a linear relation between R and the

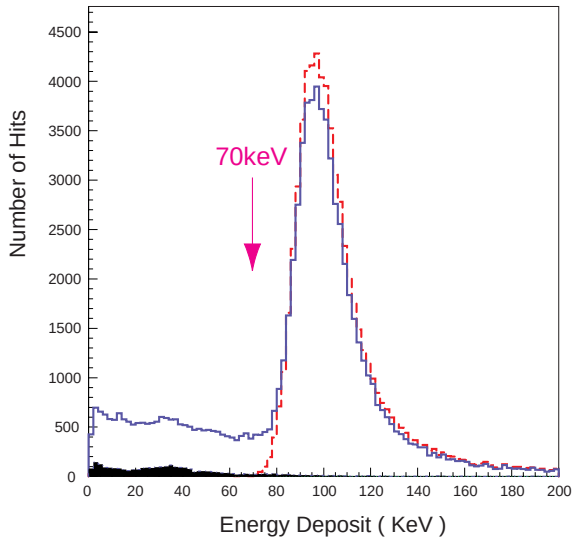

Figure 4: Energy deposits in the pair monitor. The solid and dashed histograms show energy deposits in each cell and those by a track, respectively. The black one show those of secondary backgrounds in each cell.

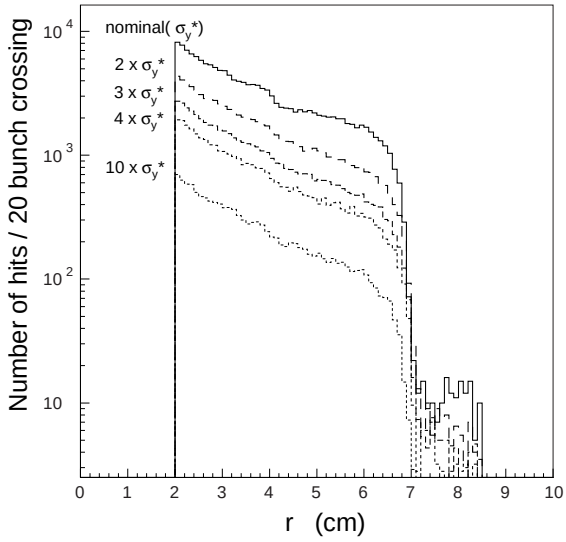

Figure 5: Hit distributions normalized at 20 bunch crossings as a function of r for energy deposits of >70keV, where histograms correspond to 5 vertical beam sizes at IP; i.e. basic (σ_y^o), $2\times, 3\times, 4\times$ and $10 \times \sigma_y^o$

.

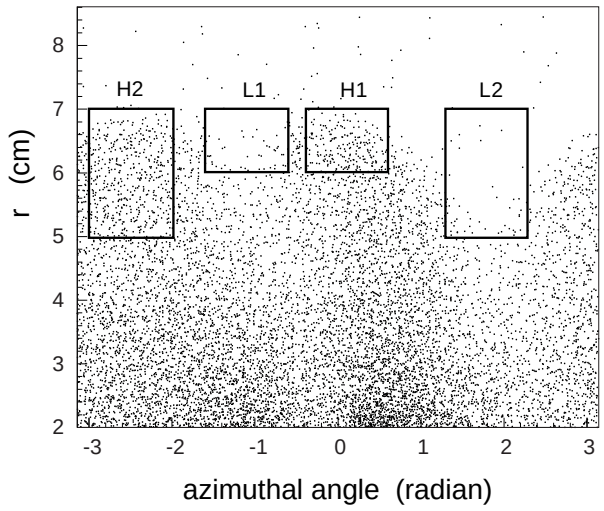

Figure 6: Scatter plot of hits with >70 keV energy deposits in the pair monitor on a plane of azimuthal angle(x) and radial position (y), where four sensitive areas are also depicted in order to calculate a ratio of $(L_1+L_2)/(H_1+H_2)$

.

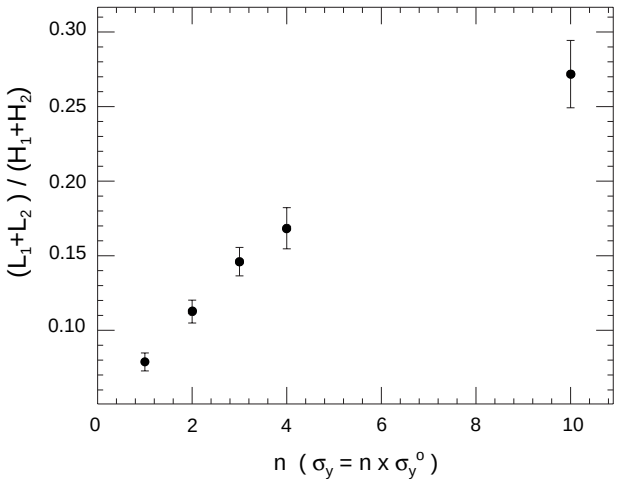

Figure 7: Ratio of $(L_1 + L_2)/(H_1 + H_2)$ as a function of vertical beam size ($\sigma_y = n \times \sigma_y^o$) at IP, where error bars are statistical corresponding to 20, 40, 60, 50 and 110 bunch crossings for n=1,2,3,4 and 10, respectively.

vertical beam size. Under the basic beam condition, the vertical beam size could be measured for 100 bunch collisions with $< 10\%$ statistical accuracy. Since this method, *i.e.* counting hit numbers in specific regions with energy deposits of greater than 70 keV, is very simple, the pair monitor can be a feedback device for beam tuning in realtime. With the fast gate, the pair monitor should detect the pairs in specific bunches in order to investigate a variance of beam size in a bunch-train.

4 "3 Tesla" v.s. "2 Tesla" for detector solenoid

There is a desire to increase the detector magnetic field (B) from 2 to 3 Tesla. The motivations are to reduce backgrounds and to place a vertex detector closer to beam line as well as to reduce the overall detector size. In this section we study a case of B=3Tesla in terms of backgrounds in two major detectors, which are a central drift chamber (CDC) filled with 1atm CO_2/isobutane (90%/10%) and a CCD vertex detector (VTX) of $25 \times 25 \mu m^2$ pixels. Inner and outer radii of the CDC are 0.45 and 2.3m, respectively, and the length is $\pm$2.3m. The VTX is assumed to be consisted of three layers (r=2.5, 5.0, 7.5 cm and z=$\pm 7.5, 15.0, 22.5$cm, respectively) in this study. Background hits were also simulated with detailed geometries by JIM, where photons and electrons(positrons) are tracked down to their energies of 10keV and 200keV, respectively.

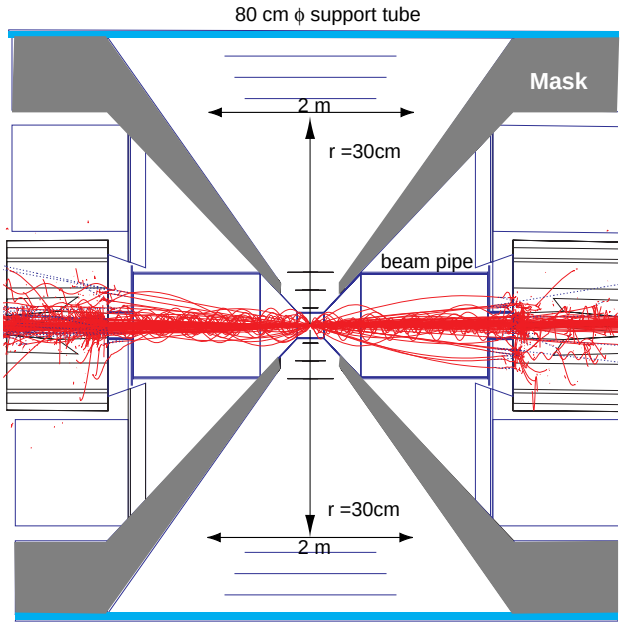

Figure 8: Pair samples in the support tube at B=2 Tesla by JIM simulation, where photons of $>$ 100MeV and electrons(positrons) of $>$ 10MeV are only shown for display purpose.

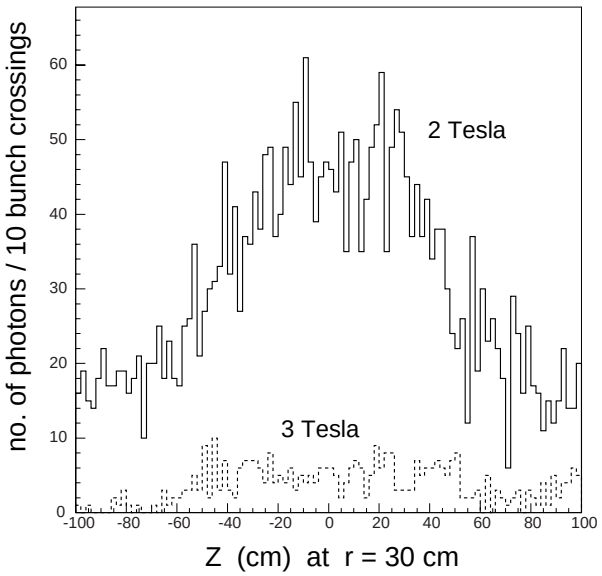

Figure 9: Number of photons traversing a cylinder of 60cm$\phi \times \pm$100cm long as a function of z at B=2 and 3 Tesla for the CDC background estimation.

The major backgrounds are secondary photons in the CDC although the CDC is shielded against them by the masks. For an estimation of the photons entering the CDC, we counted the number of photons traversing a surface of 60cm$\phi \times \pm$1m long cylinder. Figure 9 shows

Table 2: Pair backgrounds for 4cmϕ beam pipe at B=2 and 3 Tesla for beam parameters of the basic JLC-A(95 bunches/train) and the high luminosity option of JLC-Y(190 bunches/train), where numbers are for 10 bunch crossings if there is no specification.

	r	z	B = 2 Tesla		B = 3 Tesla	
	cm	cm	JLC-A	JLC-Y	JLC-A	JLC-Y
photons	30	$\pm$100	3076	6082	371	946
vtx-1:hits	2.5	$\pm$7.5	2186	3279	900	1205
/mm^2/train			0.9	2.8	0.4	1.0
vtx-2:hits	5.0	$\pm$15.0	720	920	104	306
vtx-3:hits	7.5	$\pm$22.5	406	545	34	138
CDC:hits(tracks)	45$\sim$230	$\pm$230	121(101)	235(194)	12(9)	37(28)

the results at B=2 and 3 Tesla for 10 bunch crossings. Most of the photons are created by low energy electrons (or positrons) hitting the 4cmϕ beam pipe very near IP . We can see an apparent advantage of higher magnetic field in Fig.9 because of stronger confinement of the electrons(positrons) around the beam line at B=3 Tesla. On the other hand, the main backgrounds to VTX are primary electrons(positrons).

Rates of background hits are summarized both at B=2 and 3 Tesla in Table 2. As mentioned above, the backgrounds hits in CDC are proportional to the numbers of photons, which are one order of magnitude less at B=3 Tesla than those at B=2 Tesla. The CDC hit rates were estimated to be 1210 and 120 hits per a train crossing at B=2 and 3 Tesla, respectively. Assuming that the total number of CDC readout channels is 10000, corresponding occupancy rates are 12 and 1.2 % at B=2 and 3 Tesla, respectively. In the VTX the most severe backgrounds were observed at the innermost layer, where the hit densities are estimated to be 0.9 and 0.4 /mm^2/train at B=2 and 3 Tesla, respectively. We also simulated backgrounds for the case of the high luminosity option specified as JLC-Y. The results are also listed in Table 2. For the JLC-Y, the background rates per bunch crossing increase by 1.3$\sim$3 times because of smaller beam sizes as seen in Table 1. Doubling the number of bunches per train crossing at the JLC-Y, the CDC occupancy and the VTX hit density can be estimated to be 47 (7.4)% and 2.8(1.0)/mm^2/train, respectively, at B=2 (3) Tesla.

Setting background tolerances for 10% occupancy and 1/mm^2/train hit density in the CDC and VTX, respectively, the backgrounds with B=2 Tesla are marginal at the JLC-A and they may overwhelm the detectors at the luminosity-upgraded JLC-Y. For the case of B=3 Tesla, there seems to be a possibility of placing the VTX closer to the beam line at least for the JLC-A. Therefore two configurations of the VTX and beam pipe have been studied by the JIM simulation. The first comprizes the VTX of 1.5cm minimum radius (r_{vtx1}) and 2cmϕ beam pipe, while the second comprizes the VTX of r_{vtx1}=1.8cm and 3cmϕ beam pipe. Radii of the second and third layer of the VTX are 2.5cm and 5.0cm, respectively, for both configurations. The simulation results are summarized in Table 3. From the point view of the background tolerances, the second configuration is only allowed for the CDC occupancy of 7.2% and the VTX hit density of 1.6/mm^2/train. At the JLC-Y, a more elaborate study shall be needed on a detailed geometry of beam pipe as well as a tracking algorithm in the CDC with the "exceeded" occupancy even if the innermost layer of the VTX may be overwhelmed by backgrounds.

Table 3: Pair backgrounds for 2 and 3 cmϕ beam pipes at B= 3 Tesla for the JLC-A, where numbers correspond to 10 bunch crossings if there is no specification.

	r	z	B = 3 Tesla	
	cm	cm	2cmϕ	3cmϕ
photons	30	$\pm$100	5857	1626
vtx-1:hits	1.5	$\pm$4.5	3065	-
/mm^2/train			3.6	-
	1.8	$\pm$5.4	-	1906
/mm^2/train			-	1.6
vtx-2:hits	2.5	$\pm$7.5	680	804
vtx-3:hits	5.0	$\pm$15.0	402	208
CDC:hits(tracks)	45$\sim$230	$\pm$230	259(217)	72(63)

5 Detectors at B=3 Tesla

At this workshop, K.Fujii discussed a possibility to reduce the CDC dimension by a factor of 2/3 at B=3 Tesla for preserving lepton ID momentum acceptance[10]. Since the workshop, according to the changes of the CDC dimension, detector parameters at B=3 Tesla have been proposed by each sub-detector group and individuals. To promote active discussions, all the proposed parameters are listed in Table 4 together with the standard ones at 2 Tesla, while they are very preliminary. Although there is no entree for the intermediate tracker (IT) in this table, it must be placed between the CDC and VTX. It has been emphasized that the IT should have enough number of layers, *i.e.* 4$\sim$6 layers, for self-tracking capability in order to unambiguously link a track between the CDC and VTX in the existence of many curling tracks due to pair-backgrounds[11]. The momentum resolution of the CDC itself becomes worse about twice because of shorter lever arm. However, the resolution can be recovered when the VTX and IT are taken into account in momentum reconstructions[10]. Since the degradation of momentum resolution is a major issue in this proposal, we must very carefully evaluate this performance in physics studies. For an estimation of impact parameter resolution(δ) in the VTX, the spatial resolution is set to be 4.5μm based on the beam test[12], where radiation thickness of the innermost layer including the beam pipe is assumed to be 0.55% in X_o. To improve the resolution, an effort should be made on reduction of the VTX thickness as thin as possible. Total thickness of the calorimeter increases slightly for optimization as a tile fiber readout while the overall dimension decreases[13]. The energy resolution is the same as the previous design. Finally, the detector solenoid becomes smaller by 1 and 2.3m in the diameter and length, respectively, than those of B=2Tesla[14].

6 Conclusion

Upgrade scenario for high luminosity can triple the basic luminosity at $\sqrt{s}$ =500GeV (JLC-1), *i.e.* from 0.9×10^{34} (JLC-A) to 2.6×10^{34}(JLC-Y) cm^{-2}sec^{-1}. We should prepare for such high luminosity experiment with respect to backgrounds(detectors) and physics potentials.

The IP layout was updated especially on the configuration of beam pipes and the pair monitor for background reduction in the CDC. Performance of the pair monitor has been studied by

Table 4: Major parameters of the JLC detector at B=2 and 3 Tesla,where n is a number of measured points and numbers in parentheses are constraint values with the VTX in CDC row.

		1st ACFA-LC	proposals
magnet	B (Tesla)	2	3
	size (m)	$9\phi\times$ 10	$8\phi\times$ 7.7
central	$\frac{\sigma_{P_t}}{P_t}$	$1.24(0.61)\cdot 10^{-4}P_t \oplus 0.1\%$	$2.86(0.84)\cdot 10^{-4}P_t$
tracker	type	drift chamber	drift chamber
(CDC)	n, $\sigma(\mu$m)	80, 85.	50, 85.
	size (m)	$0.45 < r < 2.3$	$0.45 < r < 1.55$
		$\lvert z\rvert < 2.3$	$\lvert z\rvert < 1.55$
electro-	$\frac{\sigma}{\sqrt{E}}(\%)$	$15/\sqrt{E}\oplus 1$	$15/\sqrt{E}\oplus 1$
magnetic	w/ scint.	tile:Pb	tile:Pb
calorimeter	size (m)	$2.5 < r < 2.7$	$1.6 < r < 1.86$
		$\lvert z\rvert < 3.5$	$\lvert z\rvert < 1.8$
	endcap	$3 < z < 3.2$	$1.9 < z < 2.16$
hadronic	$\frac{\sigma}{\sqrt{E}}(\%)$	$40/\sqrt{E}\oplus 2$	$40/\sqrt{E}\oplus 4$
calorimeter	w/ scint.	tile:Pb	tile:Pb
	size (m)	$2.7 < r < 4.0$	$1.86 < r < 3.5$
		$\lvert z\rvert < 3.5$	$\lvert z\rvert < 1.8$
	endcap	$3.2 < z < 4.8$	$2.16 < z < 3.8$
vertex	δ (μm)	$6.3 \oplus \frac{28.8}{P\sin^{3/2}\theta}$	$6.0(5.5) \oplus \frac{16.9(14.1)}{P\sin^{3/2}\theta}$
detector	type	CCD	CCD
(VTX)	size (cm)	$r = 2.4, 3.6, 4.8, 6.0$	$r = 1.8(1.5), 3.0, 4.2, 5.2$
		$\lvert z\rvert < 12.5$	$\lvert z\rvert < 10.8$

detailed JIM simulations. In this investigation, we demonstrated the ability to obtain the aspect ratio of transverse beam sizes and the horizontal beam size by measuring azimuthal angles and radial positions of pairs, respectively.

Under the background tolerances of 10% occupancy in CDC and 1 hits/mm^2/train in VTX, a configuration of (B=3 Tesla, r_{vtx1} =2.5cm) is a very secure choice both at JLC-A and JLC-Y, while configurations of (B=2 Tesla, r_{vtx1} =2.5cm) and (B=3 Tesla, r_{vtx1} =1.8cm) are marginal at JLC-A. If r_{vtx1} =1.8cm is really desired at JLC-Y, robustness of detectors against backgrounds must be verified both for the hardware and software.

For detectors at B=3 Tesla, various proposals have been presented in order to significantly reduce dimensions of detectors. We call for active discussions on such proposals. Let's define a new detector by the ACFA-LC working group toward the conceptual design.

Acknowledgments

I would like to thank all the members of ACFA-FFIR sub-group as well as the other working groups for useful discussions. I also appreciate all the participants for their stimulative discussions during this workshop. Finally, I sincerely thank the workshop organizers for their warm

hospitality and the successful workshop.

References

[1] K. Yokoya, talk presented at ACFA-LC working group meeting at KEK, March 17, 1999.

[2] JLC group, JLC-I(the green book),*KEK Report* 92-16, 1992.

[3] JLC Design Study Group: *JLC Design Study*, KEK Report 97-1, April 1997, see also ftp://lcdev.kek.jp/pub/DesignStudy/.

[4] V. Telnov, *Phys. Rev. Lett.* **78**, 4757 (1997).

[5] K.Yokoya, CAIN version 2.1d. The detailed informations can be obtained from the CAIN home page of URL = http://www-acc-theory.kek.jp/members/cain/ .

[6] T. Tauchi and K. Yokoya, *Phys. Rev.* E **51**, 6119 (1995).

[7] I. Watanabe *et al.*: $\gamma\gamma$ *Collider as an Option of JLC*, KEK Report 97-17, March 1998.

[8] T.Tauchi, proceedings of the 1st ACFA workshop on physics and detector at the linear collider (the Beijing workshop), Beijing, China, November 26-27, 1999, edited by T.Matsui and Y.Kuang, p.109, KEK Proceedings 99-12, September 1999.

[9] H.Yamaoka, in these proceedings.

[10] K.Fujii, in these proceedings.

[11] H.J.Kim, in these proceedings.

[12] Y.Sugimoto, proceedings of the Beijing workshop , p121,KEK Proceedings 99-12, September 1999.

[13] Y.Fujii, private communication.

[14] H.Yamaoka, private communication.